High temperature liquid jet fire testing

Richard. J. Alker, Senior Engineer, BAE Systems, Bridge Rd, Barrow-in-Furness LA14 1AF

Geoffrey. A. Chamberlain, Director, Waverton Consultancy Ltd, 20 Greenfield Crescent, Waverton, Chester, CH3 7NH

Abstract: Onshore oil sand extraction facilities contain large volumes of high pressure and high temperature liquid hydrocarbons. An unplanned and uncontrolled release can produce a liquid jet fire which can pose a serious hazard. To better understand the liquid jet fire and protect against it, experimental testing has been conducted. A comprehensive set of results have been obtained on the flame size and thermal properties of pentane and pentane/bitumen jet fires up to 3 kg/s release rate at simulated process conditions. These results will enable safety engineers to assess credible hazards from potential jet fires of this type and to design effective fire protection strategies.

Keywords: Liquid jet fire, cold core, pentane, solvent, solbit

Introduction

A number of oil sand facilities use high temperature and high pressure paraffinic solvents (light aliphatic hydrocarbon) for part of the bitumen extraction process. To make the process commercially viable, it is necessary to perform on a large scale where isolatable liquid hydrocarbon inventories can exceed 1000 m³. A release of solvent such as pentane or a solvent and bitumen mixture, known as solbit, can create large liquid jet fires which can be sustained for many hours. The question arises: is our understanding of liquid jet fires sufficient to cope with the hazards posed by an accidental liquid jet fire event?

There is limited published data on liquid jet fires; furthermore, there are no test standards which directly address the challenges posed by these fires. The work covered by this paper provides a detailed overview of liquid jet fire testing performed with superheated liquid pentane and solbit. Flame properties including stability, fire size, internal and external heat flux, and flame temperatures were measured for releases up to nominally 3 kg/s and compared with existing data on liquid hydrocarbon jet fires [1]. The results furthermore help to define the hazard consequences following an accidental release of solvent and the conditions that fire engulfed equipment must withstand to prevent escalation of the event.

Another reason for conducting tests was because free (non-impacting) gas jet fire stability (as seen in Figure 1 of [1]) can be misinterpreted by applying it to liquid jet fires. By claiming that free (non-impacting) liquid jet fires are unstable does not adequately address the fire hazard and the consequences to human life and asset protection. This testing has confirmed that the liquid jet fires investigated in this paper create stable jet flames.

A stable liquid jet fire contains a 'cold' core and thermal energy is required to vaporise the liquid stream. An impinged object not only experiences the lower heat fluxes associated with the cold core but also potentially higher impact pressures arising from momentum exchange at the object's surface. The implications of the cold shock and impact pressures have important considerations for the correct selection of materials for Passive Fire Protection (PFP). The existence of this cold core has been captured for what is believed to be the first time with a thermal imaging camera.

The other key differences between a liquid and gas jet fire are the mass release rate and flame shape. For a given release hole size and exit pressure, a liquid release will have a far greater mass flow rate, which significantly increases the size of the fire and resulting external thermal radiation. Also for a given hole size and exit pressure, liquid jet fires have a lower velocity than gas jet fires. The liquid jet creates a conical momentum driven region, as in a gas jet, which is approximately half the flame length. As air entrainment slows the flame, a buoyancy region becomes apparent and the flame rises upward. The relationship to momentum and buoyancy is identified in [2] and developed in [3]. The flame length is the combination of the momentum and buoyant regions.

To date, a large amount of jet fire testing was conducted around the 1990's and flame temperatures were measured using thermocouples fixed to pipe targets [1]. Internal flame temperatures were therefore limited to the target locations and it was not possible to record the temperatures throughout the entire flame. Advancements in thermal imaging technology allowed the fire tests reported here to record flame temperatures over a greater extent of the flame. Improved understanding of the flame temperature and heat flux allows for more accurate predictions of the heat up of structures and equipment. This could also have safety implications. For example, the PFP furnace test temperature maximum is around 1100°C (e.g. UL1709 or BS EN 1363-2 HC curve). A higher fire temperature would reduce the fire rated duration. For example, PFP rated to provide protection for 120 minutes may only provide protection for 90 minutes.

Experimental Procedure

Fuel and discharge orifices

Liquid jet fire testing was conducted at the Health and Safety Laboratory (HSL), Buxton, U.K, between September 2014 and February 2015. N-pentane was selected for the solvent (S) and the solbit was mixed to two solvent bitumen (B) ratios of S:B=1.4 and S:B=1.6 (by mass).

Commercial grade pentane was analysed by spiking 0.5 μl volumes of the neat sample onto two chromosorb-106 sorbent tubes. Both tubes were then analysed by thermal desorption and gas chromatography, one using mass spectrometry to identify the

components present and the second using a flame ionisation detector to obtain a quantitative analysis of the components. The result was 98.1% n-pentane, 1.6% iso-pentane and 0.3% cyclo-pentane by weight.

Bitumen was obtained from Fort Hills Energy Limited Partnership (FHELP) and contained on average 90% maltenes and 10% asphaltenes by weight. The pentane was added over a period of 5 hours. Mixture fluid temperature was maintained at $75 - 90°C$ during the mix.

The pentane and solbit were heated in a pressure vessel to a temperature between 80°C and 90°C. Nitrogen was used to maintain the pressure around 720 kPag to match typical process conditions during discharges. Three sharp edged orifices were constructed with an internal diameter of 7.1 mm, 10.0 mm and 14.1 mm giving nominally 0.7 kg/s, 1.4 kg/s and 3.0 kg/s mass flow rates. Discharge coefficients of the three orifices were measured by discharging water at a known flow rate. The values obtained were 0.635, 0.623 and 0.623 respectively. The release duration was controlled by an air actuated valve, which allowed for multiple fire tests to be conducted per batch. A strong ignition source was used consisting of a small butane jet flame (a few inches in length) located at the orifice height 1 m downstream of the horizontal release.

Instrumentation

Pressure in the solvent reservoir was measured at the vessel top and above the orifice using Druck 0-15 barg gauges. These pressures (and all other logged data channels) were logged at 1 Hz using a Biodata Microlink system. Differential pressure in the pentane feed system allowed for the calculation of flow rate and was measured using a 0-4 bar instrument supplied by Ashcroft Instruments (Model 5503). Vessel surface temperatures were measured with 0.2 mm outer diameter (o.d.) K-type thermocouples (Class 2 to BS EN 60584.3, 2008).

Temperatures in and around the jet fires were measured with 1.5 mm o.d. stainless steel sheathed, K-type thermocouples. These were supported on a water-cooled framework constructed from 1" pipes on four transverse arrays and one vertical array. Each array housed eight thermocouples. The transverse arrays were 2 m apart and at a fixed height of 3 m above grade. Initially the first transverse array was 3.7 m from the orifice, during the testing this was reduced to 2 m to immerse more of the array in the jet fire (test SC11 and onwards see Table 1). The vertical array housed thermocouples 1.75 m to 5.25 m and was positioned 6.2 m downstream of the orifice. Initially the orifice height was 3 m above grade, this was also reduced to 2 m to better utilise the horizontal thermocouple array (test SC11 and onwards). The initial position of the instrumentation can be seen in Figure 2 (SC01 to SC10) and the secondary position is shown in Figure 3 (SC11 to SC23).

Temperatures were also monitored using a thermal imaging camera FLIR SC2000 located side-on to the flame.

Bespoke internal and external heat flux gauges were designed by HSL. The principle of the heat flux gauges was to measure the rate of temperature rise of a mass of steel. For the internal heat flux gauges, a K-type thermocouple was located inside a solid steel cylinder, 50 mm in diameter and 160 mm in length. The ends of the cylinder were insulated. The external heat flux gauges were made from a steel disc, 100 mm diameter and thickness typically <6.5 mm, housed in an insulated box with the front face/steel disc exposed. A thermocouple was mounted on the back face of the disc. The heat flux detectors were painted with PNM matt black to increase the surface emissivity to $\varepsilon_s = 0.92$, calibrated by comparison with thermometric studies on standard certified paints of known emissivity. The heat flux levels Q were derived from the temperature T time series over the surface area of the discs using 12 seconds averaging as follows:

$$Q(i) = C \cdot \rho \cdot \{ T(i+6) - T(i-6)\}/12 \qquad\qquad\qquad\qquad \text{Equation 1}$$

where C is the steel disc heat capacity. Heat capacities of internal devices were derived on the basis of their dimensions, an assumed density ρ of 7800 kg/m³ and an assumed heat capacity of 490 J/kg/K. The internal flux heat gauges were mounted centrally on the 2nd and 4th transverse thermocouple arrays. Three external flux detectors were place to the side of the flame at 3 m above grade, 4.7 m downstream of the orifice at an axial distances of 5.2 m, 10.3 m and 15 m. A single axial flux detector was placed at 23.7 m from the orifice.

Other instrumentation included: a high speed optical video camera Sony XR260 High Speed - Phantom V4.1, high definition cameras Sony PMW-EX3 and a weather station Davis Model Vantage Pro.

Test Conditions

Three unignited releases of hot pentane were carried out to allow the high speed filming of the developing spray (SC01-03). These video records provided a means to establish the velocity and spread of the developing two-phase flow close to the source. A fourth unignited test (SC04) was carried out to allow filming (with the thermal camera) of the initial stages of development of a vapour cloud. One short release of hot pentane was carried out with ignition at ground level in the far field (SC05). The vapour cloud burned around the ignition source creating a local cloud fire but did not burn back to the source to form a stable jet fire.

With the ignition source repositioned 1 m downstream of the release a further twelve tests were performed with pentane and six with solbit. The test release conditions are shown in Table 1. Each fire test was approximately 60 s duration with the exception of SC20 where a suspected blockage occurred at 20 seconds. In some tests the discharge pressure could not be maintained to around the target 720 kPag and the average pressure is presented. The orifice axis direction faced SSE. Tests were performed when the

weather conditions appeared stable and relatively calm. Even so, the buoyant part of the flame was sensitive to slight wind deflections which strongly affected the results obtained from the internal instrumentation.

Table 1: Release conditions for the pentane and solbit tests

Test ID	Description	Orifice size (mm)	Pressure (kPag)	Liquid temperature (°C)	Mass flow rate at P_{av} (kg/s)	Wind and Relative Humidity
SC01	Pentane (unignited)	10.0	721	78	1.41	N <2m/s
SC02	Pentane (unignited)	10.0	734	78	1.42	N <2m/s
SC03	Pentane (unignited)	14.1	702	78	2.80	N <2m/s
SC04	Pentane (unignited)	14.1	730	78	2.86	N <2m/s
SC05	Pentane (remote ignition location)	14.1	635*	78	2.66*	N <2m/s
SC06	Pentane	10.0	738	80	1.41	N calm 60%
SC07	Pentane	7.1	670*	80	0.69*	N 0.4m/s 60%
SC08	Pentane	7.1	749	73	0.73	S 0.4 m/s 90%
SC09	Pentane	10.0	751	75	1.43	S 1 m/s 90%
SC10	Pentane	14.1	565*	80	2.45*	S 1.5 m/s 85%
SC11	Pentane	7.1	772	74	0.74	SE 0.4 m/s 87%
SC12	Pentane	10.0	791	74	1.47	SE 1.3 m/s 82%
SC13	Pentane	14.1	639*	80	2.61*	SE 1.8 m/s 82%
SC14	Pentane	10.0	715	77	1.39	SE 1.9 m/s 82%
SC15	Pentane	7.1	706	86	0.70	N 0.9 m/z 96%
SC16	Pentane	10.0	736	89	1.39	NNW 1.3 m/s 95%
SC17	Pentane	14.1	733	92	2.75	WNW 0.9-3 m/s 94%
SC18	Solbit (S:B = 1.6)	7.1	681	82	0.77	Calm 91%
SC19	Solbit (S:B = 1.6)	10.0	634	85	1.44	Calm 92%
SC20	Solbit (S:B = 1.6)	14.1	557*	88	2.68*	Calm 91%
SC21	Solbit (S:B = 1.4)	7.1	731	79	0.79	Calm 93%
SC22	Solbit (S:B = 1.4)	10.0	663	83	1.46	Calm 93%
SC23	Solbit (S:B = 1.4)	14.1	723	87	3.04	Calm 93%

*Averaged as the discharge pressure could not be maintained

Results and Discussion

The 'cold' core

The existence of this cold core of the expanding pentane and solbit jets has been captured for what is believed to be the first time with a thermal imaging camera, see Figure 1. A minimum temperature of -15°C was recorded at the first and second line of thermocouples in the unignited tests at a distance of 3.7 m and 5.7 m from the orifice (SC01 & SC02). This minimum temperature was also recorded at 7.7 m for tests SC03 & SC04 due to the higher mass flow rate. In cases where the jet was ignited the core persisted for over one hundred orifice diameters downstream. The high momentum cold core of liquid solvent centered inside the jet fire presents a novel challenge for the safe protection of nearby pipework and vessels.
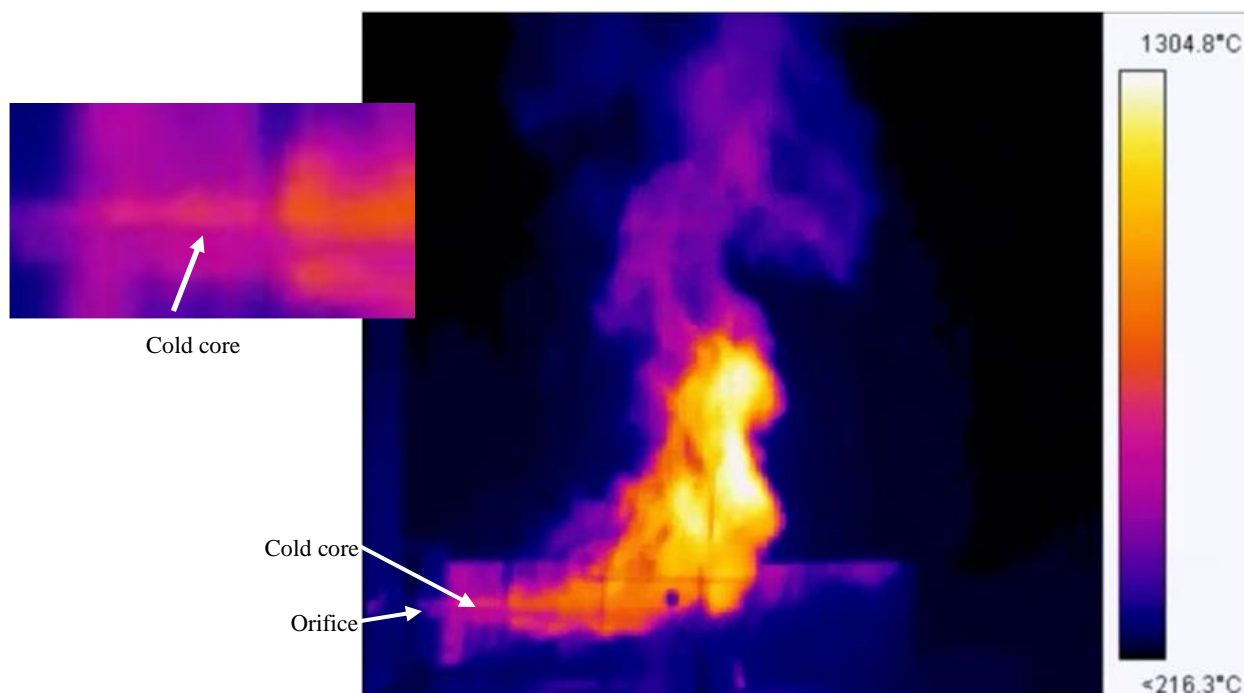
Figure 1: Thermal image of the 7.1 mm solbit release Test SC18

Jet Flame Stability

The ignition source instantly ignited the pentane and solbit releases (tests SC06+). All liquid jet fires were stable as the flame 'lift off' moved upstream from the igniter (at 1 m) to a distance of 200 mm - 400 mm (case dependent) from the orifice. This demonstrates that a liquid jet fire of pentane and solbit is stable and does not self-extinguish for the tested conditions.

Rain-Out and Smoke Formation

No rain-out was observed for the pentane jet fire releases and a small amount of smoke was observed. For the solbit tests, a very small amount of rain-out was observed. This was estimated to be less than 1 kg for each solbit batch (around 0.3% of the total charge). The solbit produced a sootier plume, and the batch with the lower S:B ratio (S:B=1.4) led to the greater amount of smoke (tests SC21 to SC23). Measurement of the smoke to determine the combustion efficiency was not made during testing.

Jet Flame Shape

The liquid pentane and solbit jet fire shapes were similar. The fire can be considered in two regions: near the release the jet is highly momentum driven and is a horizontal cone. Air entrainment reduces the velocity and the second part of the liquid jet fire is buoyancy driven. Figure 2 shows a pentane release which has a large buoyant region. The solbit jet fire displayed similar behaviour, see Figure 3. Note the change of internal instrumentation positioning and that the wind is blowing into the pentane flame, albeit at only 1 m/s, but is calm for the solbit release.

The testing observations significantly differ from the predictions of many commercial jet fire modelling software which uses a frustum of a cone to represent the liquid jet fire. This results in the model flame shape having a much greater horizontal reach. The implications are assessed later when considering the external radiation in the line of the release.
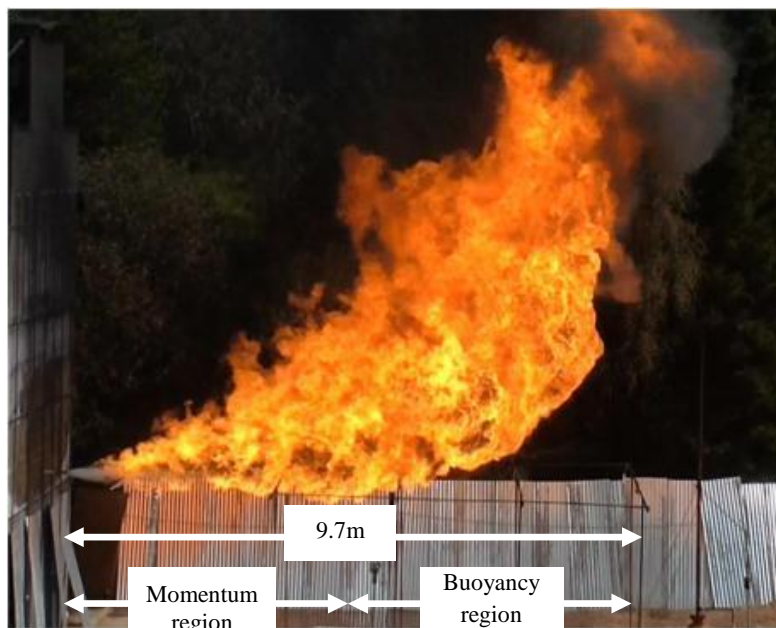
Figure 2: Liquid pentane jet fire SC09 (1.44 kg/s)

Figure 3: Liquid solbit jet fire SC22 (S:B =1.4, 1.47 kg/s)

Flame Length

The flame length was measured by considering the curvilinear length of the flame's central axis. This has been used to compare to flame lengths to a 'rule of thumb' in FABIG TN 13 [4]. The length of the jet fire, was taken from the release point to the intermittent region where flame occurrence was around 50%. The results have been time averaged for each ignited release and are presented in Table 2. The FABIG TN 13 [4] recommends that 50% flame occurrence 'rule of thumb' flame length is used for risk analysis where impingement and heat-up of equipment is concerned. For personnel, FABIG recommends that 1% should be used. There was good

agreement between the measured flame length and 50% occurrence flame length and this is evident when plotting the results of Table 2 over Figure 4.2 of [4].

Table 2: Averaged pentane and solbit flame lengths

Test ID	Material	Orifice size (mm)	Mass flow rate (kg/s)	Fire power (MW)	Curvilinear method measured (50% occurrence) (m)	FABIG rule of thumb	
						50% occurrence	1% occurrence
SC07	Pentane	7.1	0.69	31.3	11.8	10.3	12.9
SC08	Pentane	7.1	0.73	33.2	11.0	10.6	13.2
SC11	Pentane	7.1	0.74	33.7	11.6	10.6	13.3
SC15	Pentane	7.1	0.70	31.8	10.5	10.4	13.0
SC18	Solbit (1.6 S:B)	7.1	0.77	33.6	11.5	10.8	13.5
SC21	Solbit (1.4 S:B)	7.1	0.79	34.6	11.4	10.9	13.7
SC06	Pentane	10.0	1.41	63.9	12.2	13.8	17.2
SC09	Pentane	10.0	1.43	64.7	12.2	13.8	17.3
SC12	Pentane	10.0	1.47	66.4	12.7	14.0	17.5
SC14	Pentane	10.0	1.39	63.0	11.0	13.7	17.1
SC16	Pentane	10.0	1.39	63.1	13.3	13.7	17.1
SC19	Solbit (1.6 S:B)	10.0	1.44	63.1	15.1	13.9	17.4
SC22	Solbit (1.4 S:B)	10.0	1.46	63.9	15.1	14.0	17.5
SC10	Pentane	14.1	2.45	111.1	12.9	17.2	21.5
SC13	Pentane	14.1	2.61	118.1	13.0	17.6	22.0
SC17	Pentane	14.1	2.75	124.7	15.0	18.0	22.5
SC20	Solbit (1.6 S:B)	14.1	2.68	117.5	17.0	17.8	22.3
SC23	Solbit (1.4 S:B)	14.1	3.04	132.6	20.6	18.7	23.4

Flame Velocity

The unignited discharge velocity of the liquid pentane release was assessed using the high speed video camera at 1000 frames/s. The discharge velocity was measured to be around 50 m/s for the medium (10 mm) and large (14.1 mm) orifices, consistent with Bernoulli's equation of non-compressible flow. The measurement was made by tracking the progress of a turbulent structure close to the orifice: an example is provided in Figure 4. The boiling temperature of pentane is 36°C at atmospheric pressure. At 80°C to 90°C, pentane released at 720 kPag flashes after leaving the orifice as it expands to atmospheric pressure. No axial acceleration was observed, the flashing expanding radially along the jet.

The solbit releases, containing less pentane, were observed to reduce the radial expansion of the flashing jet. The result was that the momentum part of the jet extended further in a more tightly packed jet, possibly indicating a reduced rate of air entrainment. This affect is clear by comparing the horizontal reach of the base of the flame in Figure 2 and Figure 3, around 2 m for pentane and around 3 m for solbit.

For both solbit and pentane, the velocity was estimated to reduce to around 10 m/s in the buoyancy region.

Tests were typically 60 seconds in duration. On the final discharge of each batch, the pressure vessel was depressurized (emptied). After the liquid discharge, a two phase and then single phase gas discharge were observed. The discharge velocity in these cases was significantly higher than the liquid discharge and the flame lift-off point moved away from the orifice and was stabilized by the igniter. For this two phase and single gas phase release the jet fire was considered to be unstable [1] in contrast to the stable jet flame generated by the liquid jet. Nevertheless, it should be noted that the final gaseous release may have contained nitrogen.
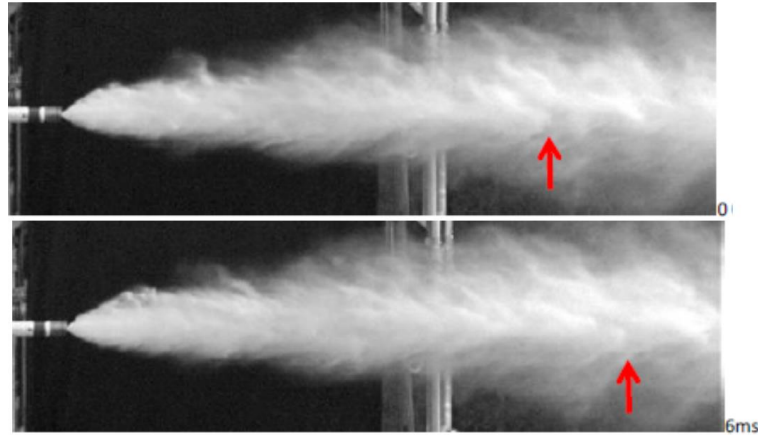
Figure 4: Test SC03 – An example of a turbulent structure in the jet convected by 231 mm in 6 ms.

Flame Temperatures

The horizontal thermocouple arrays provided a two dimensional snapshot of flame temperatures, see Figure 5. For the majority of tests, the framework array was positioned 2 m downstream and 1 m above the orifice. These thermocouples provide the internal liquid jet fire flame temperature, a means of comparing with the thermal imaging camera temperatures and also the effect of deflection of the jet flame by cross winds. The maximum temperature recorded for the pentane liquid jet fires from a thermocouple was 1170°C and 1256°C for the solbit jet fires. The issue with using thermocouples is that the temperature of the flame varies with position and it is possible that peak temperatures are not recorded. The thermal imaging camera provides a complete temperature profile throughout the entire jet fire. Although there are uncertainties in flame emissivity and partially by the atmospheric transmissivity, temperatures derived from the thermal camera at points corresponding to thermocouple locations correlated well, as shown in the example in Figure 6.
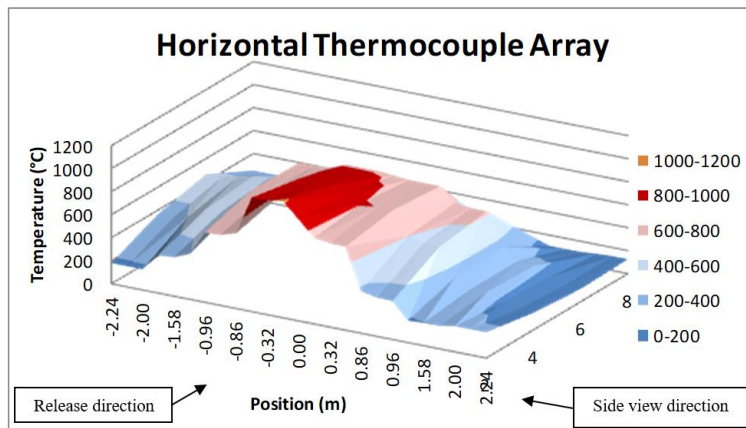

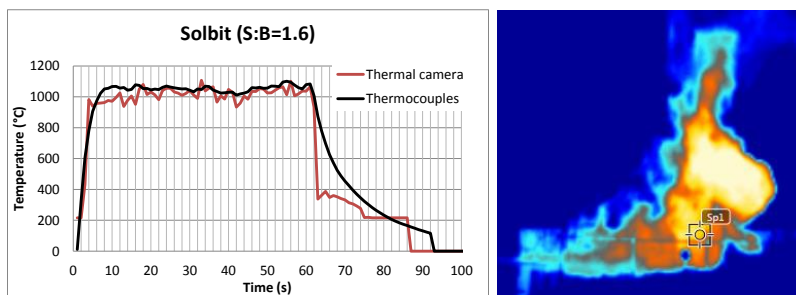Figure 5: Liquid pentane Jet Fire (2.6 kg/s) - no cross wind

Figure 6: Thermal camera and thermocouple comparison. Solbit release (S:B=1.6 test SC18).

For each jet fire, around 50 points were selected through the flame for analysis by the thermal camera. Temperatures in the high momentum region of the pentane and solbit releases were lower on account of the cold core and optically thin flame. Temperatures were observed to be hottest in the buoyancy region, but oscillations were observed due to transient hotspots. For the purpose of assessing the rate of temperature rise on structures, a time-averaged peak temperature should be used. As the convective heat flux is proportional to the temperature (Equation 3) and radiative heat flux is proportional to the temperature to a fourth power (Equation 4), the median temperature was considered more appropriate than the mean temperature. For the purpose of comparison with other fire tests a median temperature over a period of 1 second has been provided in Table 3. This data can be compared to maximum flame temperature plots in Reference [4]. To assess a more realistic heat flux on a structure a longer time-averaging period should be used. To be consistent with the dispersion time-averaging constant, the median temperature was calculated for a period of 18.75 seconds.

The thermal imaging camera provided far better and consistent data than the thermocouples due to the positioning which is evident when plotting the data of Table 3. From considering the peak time averaged temperature over 18.75 seconds, it can be seen that the temperature rises only slightly with increased mass flow rate and it is reasonable to assume that a time-averaged peak temperature around 1300°C could be achieved with larger releases. Reducing the time averaging period increases the peak temperatures and the 1 second peak temperatures are expected to exceed 1400°C for larger releases. It is useful to mention that the pentane and solbit temperatures are significantly higher than the liquid butane jet fires reported in Reference [4]. This is because the butane jet fire temperatures were measured about half way along the flame axis with thermocouples attached to a fixed pipe target and so may have missed the hottest part of the flame.

Table 3: Peak thermocouple and thermal imaging camera temperatures

Run ID	Average flow rate (kg/s)	Peak median temperature over 1 second		Peak median temperature over 19 seconds	
		Thermocouple	Thermal camera	Thermocouple	Thermal camera
SC06	1.41	1058	1274	1025	1137
SC07	0.69	1041	1201	990	1028
SC08	0.73	849	1230	815	1036
SC09	1.43	924	1316	814	1217
SC10	2.45	836	1358	774	1248
SC11	0.74	1140	N/A*	1069	N/A*
SC12	1.47	1117	1326	1073	1214
SC13	2.61	1087	1360	1054	1262
SC14	1.39	1045	1298	1015	1184
SC15	0.70	1071	1111	1016	1005
SC16	1.39	1155	1235	1072	1105
SC17	2.75	1170	1339	1152	1255
SC18	0.77	1256	1269	1223	1189
SC19	1.44	1168	1345	1129	1245
SC20	2.68	1215	1389	1169	1302
SC21	0.79	1140	1163	887	1046
SC22	1.46	1071	1200	942	1125
SC23	3.04	1208	1289	1163	1176

*Thermal imaging camera data was not recorded

Internal Heat Flux

Internal heat flux varies radially and axially along the jet flame and is a combination of radiative and convective heat transfer. As discussed later, the peak heat flux occurs within the low momentum, buoyant region of the flame. For the jet fires considered, this region is sensitive to wind deflection. Measurement of the peak internal flux is therefore difficult to achieve. Two internal gauges were used in the tests to record total heat flux by direct flame impingement. The gauges were repositioned after test SC10 in an attempt to capture a better representation of the flame heat flux, and their response was analysed over periods when the wind conditions were steady. Even so, the gauges were not generally in the hottest part of the flame. The peak heat flux measured was 191 kw/m² and recorded for the smaller jet fire size (SC11) for the internal heat flux gauge on the 2nd transversal thermocouple

array (4 m downstream and 1 m higher than the orifice). As a consequence of the limited value that could be placed on these results, calculations of the peak internal fluxes has been made by estimation of the convective and radiative components using literature data for flame velocities and flame temperatures derived from the thermal camera trained on the hot and optically thick buoyant portion of the flame.

The convective heat flux depends on the flow speed and temperature of the gas at a target. The flow velocity at a point in the buoyant region for a 50-100 MW fire is about 10 m/s. The heat transfer coefficient h (in the buoyant region) was estimated to be around 42 W/m²/K for a 50 mm cylinder in a cross flow orientation and in dry air using the relationship between the Nusselt, Reynolds and Prandtl numbers [6] given by:

$$\overline{Nu_D} = CRe_D^M Pr^{1/3}$$

Equation 2

where the constants C and M are 0.193 and 0.618 respectively at a Reynolds Number of 4×10^4 to 4×10^5 [5].

The presence of water vapour changes the gas properties (from dry air). Therefore, an approximate value of $h = 50$ W/m²/K has been used in the buoyancy region in an attempt to overcome the uncertainty of the velocity and the presence of water vapour.

The convective heat flux load Q_{con} per unit area for initial flame impingement of temperature T_f on a target surface at temperature T_s can then be calculated from:

$$Q_{con} = h\left(T_f - T_s\right)$$

Equation 3

The radiative heat flux load Q_{rad} per unit area can be calculated from the following equation, where the Stefan-Boltzmann constant, $\sigma = 5.67 \times 10^{-8}$ W/m²/K⁴, and ε_f is the flame emissivity.

$$Q_{rad} = \sigma \varepsilon_f T_f^4$$

Equation 4

The total thermal load to the target is therefore the sum of these two components.

For large sooty flames such as those considered here the flame emissivity approaches unity [5]. Assuming that the target is initially cold (near or just above room temperature) relative to the flame then the convective heat flux per unit area may be estimated. Conversely, knowledge of the heat transfer coefficient, flame temperature and emissivity can be used to calculate the initial total heat flux absorbed by a target and enable heat-up calculations to determine the temperature rise with time.

In the momentum region the average axial temperature increases with distance from the release point and the velocity reduces. The overall effect is that the heat flux increases with distance and the greatest heat fluxes are observed in the buoyancy region. However, the contributions made by the convective and radiative components change along the flame. In the momentum region of the liquid jet flame the contributions may be roughly equal, but in the buoyant region the radiation component clearly dominates. In the cold core region near the release orifice the initial heat transfer may even be from target to jet, with the low temperature high velocity stream imparting large stresses. These considerations are important factors when considering the use of PFP to protect equipment and the suitability of existing test methods such as ISO22899-1 [7]. A gas jet fire displays generally different behaviour. For instance, the maximum heat fluxes have a higher convective component.

The heat fluxes per unit area calculated for the buoyancy region of the tested liquid jet fire are provided in Table 4. The flame temperatures were averaged from Table 3 for the thermal camera with 18.75 s time averaging. It can be seen that the thermal load continues rising with the mass release rate for both pentane and solbit. Therefore, for larger releases it is reasonable to assume that this thermal load will rise above 300 kW/m² which is the maximum reported in ISO22899-2 [8] for a 0.3 kg/s propane gas jet fire. This exceeds current jet fire testing and also furnace testing temperature (e.g. UL 1709 or BS EN 1363-2 HC curve). Note that the radiant load has been calculated for a black body and a reduction can be taken into account when calculating the load to a grey body with an emissivity less than unity.

Table 4: Peak averaged pentane and solbit maximum heat fluxes per unit area, calculated from the flame temperature assuming the flame emissivity is unity

Hydrocarbon	Orifice size (mm)	Mass flow rate (kg/s)	Fire power (MW)	Average flame temperature (°C)	Thermal load (kW/m²)		
					Qrad	Qcon*	Total
Pentane	7.1**	0.71	32.0	1023	160	48	208
	10	1.42	64.1	1171	247	56	302
	14.1	2.59	117.0	1255	309	60	369
Solbit	7.1	0.78	34.0	1117	212	53	265
	10	1.45	63.2	1185	256	56	313
	14.1	2.84	124.1	1239	297	59	356

*Target temperature, Ts, assumed to be 60°C.
** SC11 excluded as the thermal imaging camera was not available for this test.

External Heat Flux and Surface Emissive Power

The external heat flux was measured using four heat flux gauges. Distance of the flame centre from each gauge was corrected for wind deflection of the flame axis by correlation with the maximum temperatures measured at the transverse thermocouple arrays. The height difference between the centre of the flame and the flux detectors was also taken into account when calculating the distance commonly defined in point source models as radius 'r'. The method of determining the position is approximate as the horizontal thermocouple array was positioned below the centre of the fire and under-predicts the effects of cross wind. The results for the large orifice releases are shown in Figure 7.

The small and large release have been plotted on a logarithmic scale in Figure 8 and Figure 9. A point source model with 25%, 35% and 50% radiative fraction has also been plotted. The heat fluxes vary as $1/r^2$ for values of heat flux less than about 30 kW/m². Above 30 kW/m² the point source model becomes increasingly inaccurate and a view factor model is more appropriate. The fraction of heat radiated from the small orifice was estimated to be 0.38 ± 0.05. This reduced to around 0.25 ± 0.05 for the large orifice. This change is believed to be caused by the method calculating the receiver distance and reduced obscuration by smoke for the larger fire power. There appeared to be no significant difference between solbit and pentane flame radiation even for the higher bitumen loadings in tests SC21-SC23 with the exception of SC13 which was subject to higher wind speeds affecting the buoyant region of the flame.
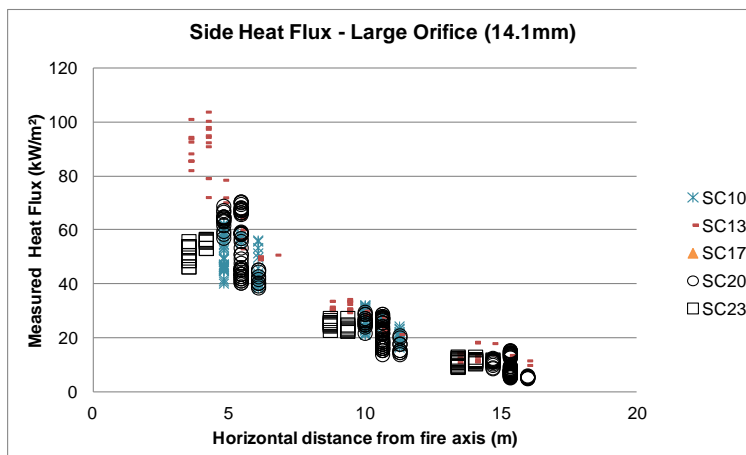

Figure 7: Incident radiation data for the large orifice tests. The variation in distance is the correction for wind deflection of the flame axis.
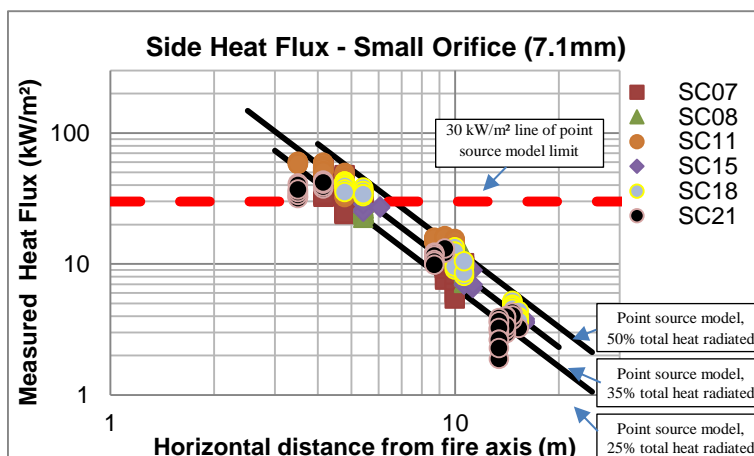
Figure 8: Functional dependence of radiation flux on distance ($\sim 1/r^2$ at large distance) for the small release. The straight lines are calculations based on a point source model.
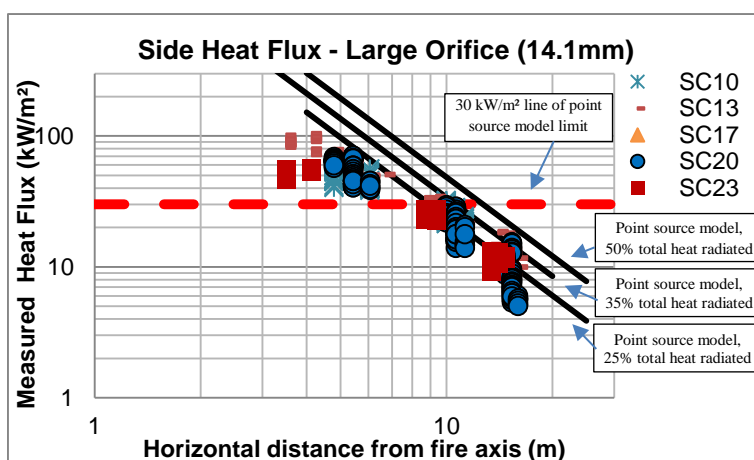
Figure 9: Functional dependence of radiation flux on distance ($\sim 1/r^2$ at large distance) for the large release. The straight lines are calculations based on a point source model

The reduction in radiative fraction with mass flow rate is similar to that in pool fires. As the pool fire diameter increases above about 4 m (about 50 MW), the effective radiative fraction starts to fall, caused by increased obscuration of the upper parts of the flame by soot. A release rate of 2.68 kg/s (average for the large orifice) corresponds to the heat release from a 6.3 m diameter pool fire. Pool fires of this size have a radiative fraction of about 0.24 [9] which aligns well with the results in Figure 9.

The average Surface Emissive Power (SEP) for the entire flame was calculated from the side view flux detectors. This was achieved by taking account of the flame view factors (by dividing the flame image into rectangles), atmospheric transmissivity and distance between the flame and each flux detector. The derived average SEP for the pentane tests was around 200 kW/m², and 180 kW/m² for the solbit tests, again indicating some obscuration by smoke over the solbit flame surface. The slightly lower SEP for solbit is offset by the slightly longer flames resulting in a similar external radiation flux compared with pentane.

The axial heat flux was measured at 24 m (downstream and inline) of the release. To minimise fluctuations the heat flux was averaged over 19 seconds (see the flame temperature section). The averaged axial heat fluxes has been plotted in Figure 10 (labelled pentane/solbit test average).The axial heat flux for each test has also been plotted at 5 second intervals in Figure 10 (labelled pentane/solbit). Note that tests SC17 and SC18 were excluded due to high cross winds and instrumentation issues respectively.

As discussed earlier in the paper, the jet flame shape is made up of a momentum and buoyancy region. As expected, the fire power was sensitive to wind as the axial heat flux emanates from the buoyancy region of the fire. It was also observed that for

the large orifice (14.1 mm) at higher pressures, greater flame lengths were achieved which reduced the separation between the fire and the flux detector. This indicates the importance of correctly modelling the momentum and buoyancy regions. Jet fire modelling software that uses a frustum of a cone to represent a horizontally released liquid jet fire can grossly over-predict the axial heat flux. This can have significant implications on quantitative risk assessments, facility siting and application of PFP.

Figure 10: Measured Heat Flux 24 m downstream and inline of the Orifice

Conclusion

Superheated, pressurised and horizontal releases of liquid pentane and pentane/bitumen (solbit) up to 3 kg/s are easily ignited and form stable jet fires. Under test conditions of around 720 kPag and 80°C there was little or no rain-out.

Near the release orifice, the jet velocities reached a maximum of about 50 m/s and consisted of a cold core of evaporating droplets which expanded radially. At distances greater than about half a flame length, flow speeds in the jet were low and of the order 10 m/s. The flames rose upwards as a result of buoyancy and were easily deflected by light winds. As such, commercial jet fire modelling software which uses a frustum of a cone to represent the horizontally released liquid jet does not capture the profile which can result in under-predicting the external side heat flux and may grossly over-predicting the downstream heat flux thereby impacting on safety and cost.

The heat flux and temperature in the buoyant part of the jet flame were some of the highest ever recorded for a liquid jet fire. Internal heat fluxes were dominated by radiation. Maximum values of around 190 kW/m² were recorded by fixed flux detectors but these devices were not in the hottest parts of the flames. Thermocouple measurements and thermal imaging suggest that there are areas of the flame, where the radiant intensity in the flame would be a maximum of about 310 kW/m². Convective heating to a cold surface could add another 60 kW/m². It is expected that the heat flux could be slightly greater with larger releases. The higher temperatures and heat fluxes help to more accurately predict the performance of PFP influencing facility design and emergency response arrangements.

External radiative heat flux data do not show any marked differences between pentane and solbit flames in similar conditions. Measurements at long range suggest that the proportion of the total heat release appearing as thermal radiation was similar to that in pool fires of comparable size i.e. 25% to 35%.

Acknowledgment

FHELP is formed of Suncor Energy, Teck Resources and Total. FHELP sponsored this work and agreed to share the research to further industry understanding and increase safety for the wider community. We would like to especially thank Shawn van der Merwe and Bryan Demko (Suncor) for their tremendous insight, technical prowess and support making this work possible. We thank Graham Atkinson and Health and Safety Laboratory for their expertise and for conducting the liquid jet fire testing and we acknowledge Atkins for their role in facilitating the test.

Acronyms

FHELP	Fort Hills Energy Ltd Partnership
HSL	Health and Safety Laboratory
PFP	Passive Fire Protection
SEP	Surface Emissive Power
S:B	Solvent to Bitumen ratio

References

1   Lowesmith, B., Hankinson, J., Acton, R. and Chamberlain, G., 2007, An overview of the nature of hydrocarbon jet fire hazards in the oil and gas industry and a simplified approach to assessing the hazards, Trans. I chem. E Part B, Process Safety and Environmental Protection, 85(B3), 207-220.

2   Brightwell, H., and Carsley. A., 1994, A model for predicting the thermal radiation hazards from large-scale horizontally released natural gas jet fires, A.D. Johnson, I Chem E Symposium Series No. 134.

3   Carsley, A., 1995, A model for predicting the probability of impingement of jet fires, I Chem E Symposium Series No. 139.

4   Design Guidance for Hydrocarbon Fires, FABIG Technical Note 13, 2014.

5   Drysdale, 1985, An Introduction to Fire Dynamics, Pub John Wiley.

6   Incropera & De Witt, 1981, Fundamentals of Heat and Mass Transfer, Pub. John Wiley.

7   Determination of the resistance to jet fires of passive fire protection material, BS ISO22899-1:2007, Part 1: General Requirements.

8   Determination of the resistance to jet fires of passive fire protection material, BS ISO22899-2:2013, Part 2: Guidance on classification and implementation methods.

9   McGrattan, K., Baum H. R., and Hamins, A., 2000, Thermal Radiation from Large Pool Fires, NISTIR 6546.